Formation of a crystal of Brownian particles under a uniform external force

Masahide Sato*
Information Media Center, Kanazawa University, Kakuma-machi, Kanazawa 920-1192, Japan

Hiroyasu Katsuno
Computer Centre, Gakushuin University, 1-5-1 Mejiro, Toshsima-ku, Tokyo 171-8588, Japan

Yoshihisa Suzuki
Department of life system, Institute of Technology and Science, The University of Tokushima, 2-1, Minamijosanjima, Tokushima, Tokushima 770-8506, Japan

(Received 20 December 2012; revised manuscript received 9 February 2013; published 18 March 2013)

To keep the formation of colloidal crystal under a centrifugation in mind, we study ordering of Brownian particles under a uniform external force. When the force is added to Brownian particles distributing uniformly in the system, the particles drift and the density of particles near walls increases. Ordering of particles on the walls occurs at first and ordering in bulk occurs in succession. In bulk, both the clusters with face-centered cubic structure and those with the hexagonal close-packed structure appear. The distribution of cluster sizes changes with the direction of external force.

DOI: 10.1103/PhysRevE.87.032403 PACS number(s): 82.60.Nh, 82.70.Dd, 61.50.−f

I. INTRODUCTION

A close-packed colloidal crystal with the face-centered cubic (fcc) lattice is one of coordinates of a three-dimensional photonic crystal. If the close-packed crystal without defects is formed, we can use the colloidal crystal as a template for inverse opals with perfect three-dimensional photonic band gaps [1], which is used to produce optical integrated circuits [2]. Now, the optical integrated circuits with a large size have not been produced yet, but if we succeed in forming a large size of inverse opals with perfect three-dimensional photonic band gaps, it may be possible to produce a lot of large optical integrated circuits from an inverse opal at a time. Thus, to use colloidal crystals as device applications, we need to create a large size of crystal without defects.

If our purpose is only to create a large colloidal crystal quickly, it is better to intend to create a non-close-packed colloid crystal [3–6]. However, the non-close-packed colloidal crystals cannot be used as a template for inverse opals, so we need to create large close-packed colloidal crystals for optical integrated circuits. One of approaches to creating a close-packed colloidal crystal with few defects is epitaxial growth on a patterned substrate. Using a template with a regular array of pyramidal pits, Yin and co-workers [7] tried to form a large colloidal crystal without defects, but the colloidal crystal they obtained was so thin that it is necessary to increase the thickness of the crystal. Another approach to creating a close-packed colloidal crystal is to use sedimentation by gravitation. Davis and co-workers [8] succeeded in creating a thick colloidal crystal, but the colloidal crystal they created was a narrow columnar crystal. If the area of the base of a columnar crystal can be spread, the use of gravitational force may be a good method to form large colloidal crystal.

From simulations of hard sphere particles [9,10], it was shown that well-ordered crystals are formed by controlling the sedimentation force. In experiment [8], however, controlling the sedimentation force is difficult and the number of nuclei, which determines the final number of columnar grains, is hardly controlled. To solve the problems in the experiment [8], recently, Suzuki and co-workers [11,12] used a centrifugation method and succeeded in forming large three-dimensional colloidal crystals controlling the size of the grain. In Ref. [12], they used in an inverted-triangle internal-shaped container (inverted-triangle container) and showed that the grain size of a colloidal crystal becomes larger than that produced in a container with a flat bottom. When a flat-bottomed container is used, the centrifugation force is perpendicular to a wall. The nucleation of colloidal crystal occurs in various places on the wall and small grains are formed. However, when an inverted-triangle container is used, the nucleation mainly occurs on the edges or in a corner of the container and the number of nuclei formed in an early stage decreases. In Ref. [13], the effect of the wall during nucleation in pores was studied. It is shown that nucleation easily occurs at a corner of the walls. In the system [12], particles are gathered around walls by a centrifugal force and nucleation occurs from a wall. By changing the form of the container, the place where the nucleation of colloidal crystal is controlled. The addition of the centrifugal force provides a setup slightly different from a previous study [13], but the wall there as well probably plays an important role.

In this paper, to keep the results of the experiments [11,12] in mind, we carry out a Brownian dynamics simulation and study how the formation of colloidal crystal is affected by the direction of force. In Sec. II, we introduce our model. In Sec. III, we show the results of our simulation. We investigate some order parameters and show that the process of crystallization depends on the direction of the external force. In Sec. IV, we summarize our results and give brief discussions.

II. MODEL

The system we use is a cuboid whose size is given by $L_x \times L_y \times L_z$. In the y direction, we use a periodic boundary

*sato@cs.kanazawa-u.ac.jp

condition. We consider hard flat walls in the x and z directions. We assume that the particles act as hard sphere particles for the walls, so that perfectly elastic collision between walls and the particles occurs at the walls. We use N sphere colloidal particles whose mass is m. In general, the motion of the ith particle is given by

$$m\frac{\mathrm{d}^2\boldsymbol{r}_i}{\mathrm{d}t^2} = \boldsymbol{F}_i - \zeta\frac{\mathrm{d}\boldsymbol{r}_i}{\mathrm{d}t} + \boldsymbol{F}_i^{\mathrm{B}}, \tag{1}$$

where $\boldsymbol{r}_i$ is the position of the ith particle, $\boldsymbol{F}_i$ is the sum of an external force and the force from other particles, and ζ is the frictional coefficient. $\boldsymbol{F}_i^{\mathrm{B}}$ is the random force satisfying $\langle \boldsymbol{F}_i^{\mathrm{B}}(t)\rangle = \boldsymbol{0}$ and $\langle F_{ix}^{\mathrm{B}}(t)F_{ix}^{\mathrm{B}}(t')\rangle = \langle F_{iy}^{\mathrm{B}}(t)F_{iy}^{\mathrm{B}}(t')\rangle = \langle F_{iz}^{\mathrm{B}}(t)F_{iz}^{\mathrm{B}}(t')\rangle = 2\zeta k_{\mathrm{B}}T\delta(t-t')$, where T is temperature and k_{B} is the Boltzmann constant. The force $\boldsymbol{F}_i$ is given by

$$\boldsymbol{F}_i = F_{\mathrm{ext}}\mathbf{e}_{\mathrm{ext}} + \sum_{i\neq j}\boldsymbol{F}_{ij}, \tag{2}$$

where the first term is the external force by centrifugation and the second term is the force from other particles. F_{ext} and $\boldsymbol{e}_{\mathrm{ext}}$ represent the strength and the direction of the external force, respectively. By using the interaction potential $U(r_{ij})$, the force from the jth particle is given by $\boldsymbol{F}_{ij} = -\nabla U(r_{ij})$, where $r_{ij} = |\boldsymbol{r}_{ij}| = |\boldsymbol{r}_i - \boldsymbol{r}_j|$ is the distance between the two particles. For simplicity, we take account of a short- range interaction and use the Weeks-Chandler-Anderson potential [14] as $U(r_{ij})$. Namely, $U(r_{ij})$ is expressed as

$$U(r_{ij}) = \begin{cases} 4\epsilon\left[\left(\frac{\sigma}{r_{ij}}\right)^{12} - \left(\frac{\sigma}{r_{ij}}\right)^{6} + \frac{1}{4}\right], & (r \leqslant r_{\mathrm{in}}), \\ 0, & (r \geqslant r_{\mathrm{in}}), \end{cases} \tag{3}$$

where σ represents the diameter of particles and $r_{\mathrm{in}} = 2^{1/6}\sigma$.

We assume that the viscosity is high. The acceleration rate is so slow that the left-hand-side term in Eq. (1) is neglected. The velocity is approximately given by

$$\frac{\mathrm{d}\boldsymbol{r}_i}{\mathrm{d}t} = \frac{1}{\zeta}\left(\boldsymbol{F}_i + \boldsymbol{F}_i^{\mathrm{B}}\right). \tag{4}$$

In our simulation, we use σ, $\zeta\sigma^2/\epsilon$, and ϵ/σ as the units of length, time, and force, respectively. The normalized difference equation of Eq. (4) is expressed as [15]

$$\tilde{\boldsymbol{r}}_i(\tilde{t}+\Delta\tilde{t}) = \tilde{\boldsymbol{r}}_i(\tilde{t}) + \tilde{\boldsymbol{F}}_i\Delta\tilde{t} + \Delta\tilde{\boldsymbol{r}}_i^{\mathrm{B}}, \tag{5}$$

where $\tilde{\boldsymbol{r}}_i = \boldsymbol{r}_i/\sigma$ $\tilde{t} = t\epsilon/\zeta\sigma^2$, and $\tilde{\boldsymbol{F}}_i = \boldsymbol{F}_i\sigma/\epsilon$. The scaled displacement of the ith particle by the random force, $\Delta\tilde{\boldsymbol{r}}_i^{\mathrm{B}}$, satisfies $\langle\Delta\tilde{\boldsymbol{r}}_i^{\mathrm{B}}(t)\rangle = \boldsymbol{0}$ and $\langle\Delta x_i^{\mathrm{B}}(t)\Delta x_i^{\mathrm{B}}(t')\rangle = \langle\Delta y_i^{\mathrm{B}}(t)\Delta y_i^{\mathrm{B}}(t')\rangle = \langle\Delta z_i^{\mathrm{B}}(t)\Delta z_i^{\mathrm{B}}(t')\rangle = 2\tilde{R}^{\mathrm{B}}\Delta\tilde{t}$, where $\tilde{R}^{\mathrm{B}} = k_{\mathrm{B}}T/\epsilon$.

III. RESULTS OF SIMULATION

Initially, we put particles at random and relax the position of particles without an external force for sufficiently long time. Then, we add an external force and move particles. In all simulations, the displacement by random force, $\tilde{R}^{\mathrm{B}}$ is 0.1, the time step $\Delta\tilde{t} = 4.0\times10^{-4}$, and the strength of the force $\tilde{F}_{\mathrm{ext}} = 1.0$. Since the drift velocity is F_{ext}/ζ and the self-diffusion coefficient $D = k_{\mathrm{B}}T/\zeta$, the Peclet number $\mathrm{P_e}$ is given by

$$\mathrm{P_e} = \frac{F_{\mathrm{ext}}\sigma}{k_{\mathrm{B}}T} = \frac{\tilde{F}_{\mathrm{ext}}}{\tilde{R}_{\mathrm{B}}} = 10.0, \tag{6}$$

which is much larger than the value used in some previous studies [16–19].

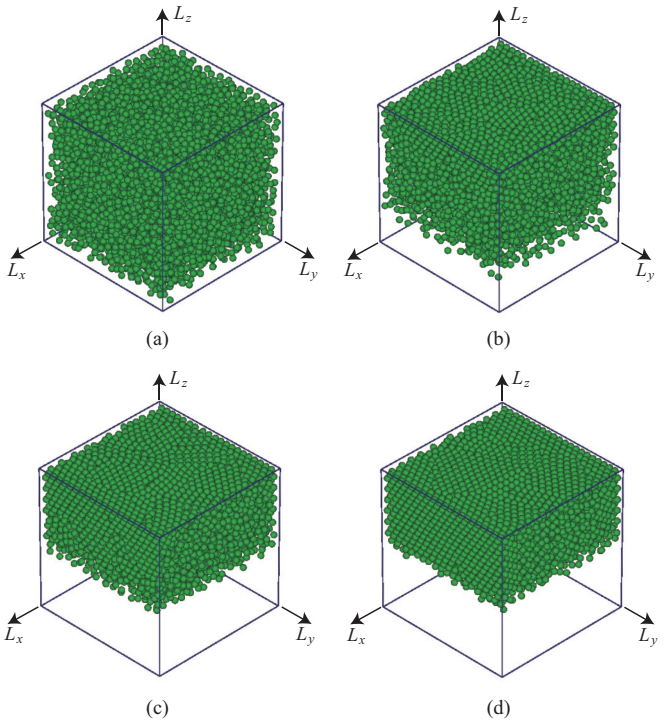

FIG. 1. (Color online) Snapshot of particles with various times. Number of particles N is 6912, and system size is $L_x/\sigma = L_y/\sigma = L_z/\sigma = 23$. External force is given by (0,0,1). Times are (a) $\tilde{t} = 0.4$, (b) $\tilde{t} = 6.0$, (c) $\tilde{t} = 12.0$, and (d) $\tilde{t} = 80.0$.

Figure 1 shows the time evolution of crystallization with external force (0,0,1) and $(1,0,1)/\sqrt{2}$, respectively. The particles are initially put in the system at random [Figs. 1(a)]. Then, we add the uniform external force. Since the force is in the z direction, the particles start gathering to the upper side [Fig. 1(b)]. The density of particles at the upper wall increases and ordering of particles on the wall occurs at first. Then, the width of the ordered region increases [Figs. 1(c)–1(d)]. Figure 2 shows snapshots of crystallization of particles with a tilting force $(1,0,1)/\sqrt{2}$. In a very early stage [Fig. 2(a)], the distribution of particles is the same as that in Fig. 1(a). Since the external force is tilted, particles start moving to the edge between two walls $x = L_x$ and $z = L_z$ [Fig. 2(b)]. With increasing time, the density of particles around the edge becomes high and ordering on the two walls starts around the edge [Fig. 2(c)]. In the last stage [Fig. 2(d)], all the particles gather obliquely upward. With a small wall, a square lattice is sometimes preferred [9,20], but our system is not so small. Since particles are pressed to walls by the external force and the pressure from other particles, the density of particles on walls tends to become high and the triangle lattice is expected to be formed on the wall.

At a glance, we cannot judge which is more ordered, Fig. 1(d) or Fig. 2(d). To estimate ordering of particles on

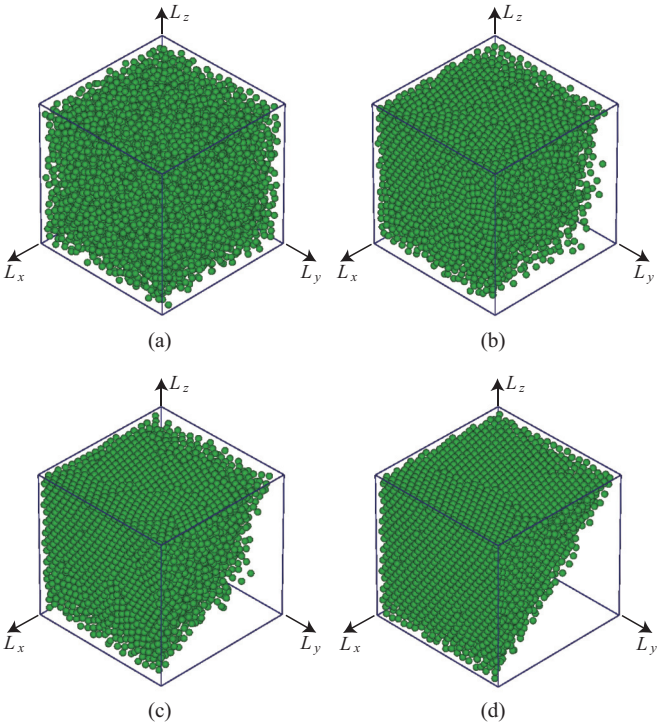

FIG. 2. (Color online) Snapshot of particles with various times. Number of particles N is 6912, and system size is $L_x/\sigma = L_y/\sigma = L_z/\sigma = 23$. External force is given by $(1,0,1)/\sqrt{2}$. Times are (a) $\tilde{t} = 0.4$, (b) $\tilde{t} = 6.0$, (c) $\tilde{t} = 12.0$, and (d) $\tilde{t} = 80.0$.

walls quantitatively, we calculate a sixfold orientation order variable. The orientation order around the kth particle, ψ_k, is defined as [21]

$$\psi_k = \frac{1}{n_k}\left|\sum_{m=1}^{n_k} \mathrm{e}^{6\mathrm{i}\theta_{km}}\right|, \tag{7}$$

where n_k is the number of neighboring particles of the kth particle. When the distance between a particle and a wall is smaller than $r_{\mathrm{in}}/2$, we regard the particle as attaching on the wall. In calculating Eq. (7), we take account of the particles attaching on the wall. If $|\boldsymbol{\rho}_{km}| = |(x_{km}, y_{km})|$, where x_{km} and y_{km} are the x and y components of the distance between the mth particle and the kth particle, is smaller than $1.2r_{\mathrm{in}}$, we treat the mth particle as a neighboring particle [22–24]. θ_{km} is the angle between $\boldsymbol{\rho}_{km}$ and the edge between the walls $x = L_z$ and $x = L_x$. Figure 3 shows snapshots of the top wall in Fig. 1. We regard the particles with $\psi_k > 0.9$ as ordered particles and color them in Fig. 3. If the ordered particles line parallel to the edge between the walls $x = L_x$ and $z = L_z$ (the edge given by $x = L_x$ in Fig. 3), we color them in red (dark gray). With increasing the angle of the line of particles from the edge between the walls $x = L_x$ and $z = L_z$. We gradually change the color. The color becomes yellow (light gray) when the angle is 30°. Owing to the sixfold orientation order, the color returns to red when the angle is 60°. The particles with $\psi_k < 0.9$ are regarded as disordered ones and we color them white. Green (dark) particles are the particles which do not attach to the walls.

The upper wall, which is given by $z = L_z$, is filled with a lot of particles at a time in an early stage [Fig. 3(b)]. The

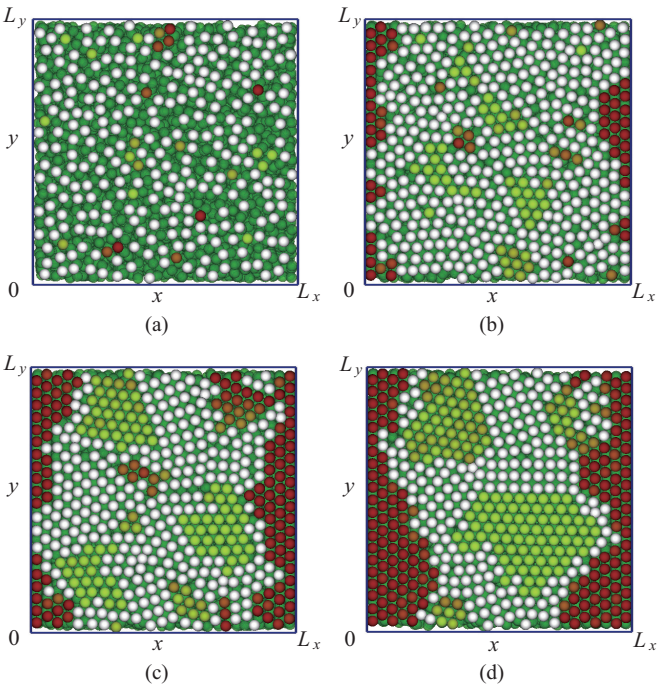

FIG. 3. (Color online) Snapshot of particles on the $z = L_z$ wall. Particles with local sixfold orientational symmetry are colored. Red (dark gray) particles line parallel to the y axis. With increasing the rotating angle, the color gradually changes. When the rotating angle is 30°, the particles are colored yellow. Times of (a)–(d) are same as those in Figs. 1(a)–1(d).

ordered particles with the rotating angle 0° appear around two sides $x = 0$ and $x = L_x$, and small islands of the ordered particles with the rotating angle 30° appear at the center of the top wall. In Fig. 3(c), ordering of particles along the two sides proceeds, and the area of ordered islands appearing at the center of the wall increases. In the final stage [Fig. 3(d)], thick layers of red ordered particles are formed on the two sides and large islands of yellow ordered particles appear at the center of the upper wall. In addition to the region with the sixfold orientational symmetry, some white particles seem to produce a square lattice structure.

Ordering on walls is changed by the direction of the external force. Figure 4 shows the time evolution on the wall $x = L_x$ where the external force is perpendicular to the normal direction of the wall. In the initial stage [Fig. 4(a)], although the density of particles attached on the wall $x = L_x$ is slightly smaller than that on the wall $z = L_z$, the distribution of particles is similar to that on $z = L_z$. However, the process of ordering on $x = L_x$ is different from that on $z = L_z$. In an early stage [Fig. 4(b)], the number of particles attached on the wall starts increasing from the upper side, and ordered particles appear in the region with high density. In the ordered regions, the rotating angle from the edge at $z = L_z$ is 0°. The width of the ordered region increases and thin layers are formed. [Fig. 4(c)]. The width of the layer gradually increases with time. Small ordered regions with the rotating angle 30° are temporally formed during ordering, but the regions do not grow and vanish. In the final stage [Fig. 4(d)], almost all of the particles are ordered with rotating angle 0°. Although ordering on the wall $z = L_z$ seems to be better than that on the

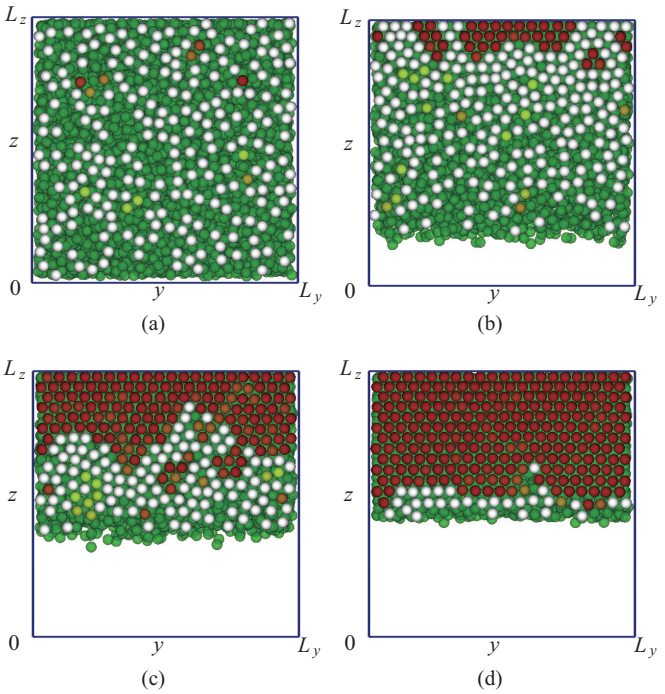

FIG. 4. (Color online) Snapshots of particles on the $x = L_x$ wall. Particles with local sixfold orientational symmetry are colored. The meaning of the colors of the particles is the same as that in Fig. 3. Times of (a)–(d) are the same as those in Figs. 1(a)–1(d).

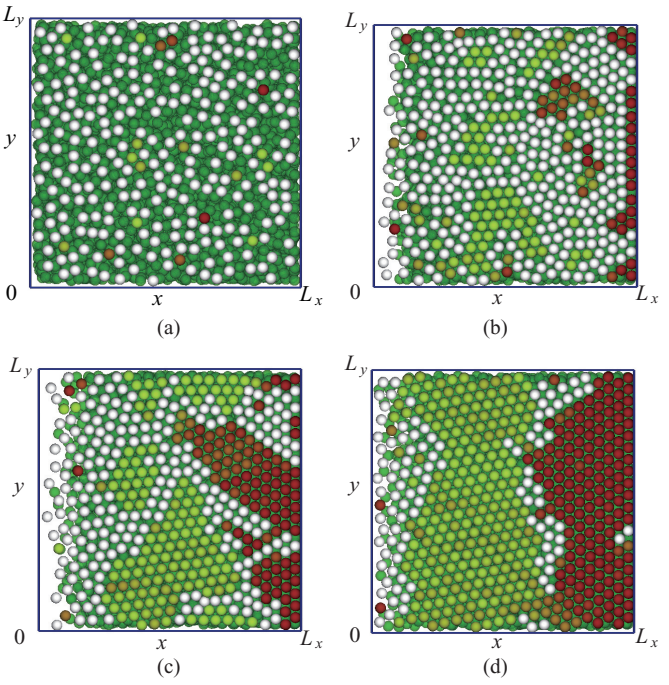

FIG. 5. (Color online) Snapshot of particles on the $z = L_z$ wall with the force $(1,0,1)/\sqrt{2}$. Particles with local sixfold orientational symmetry are colored. The meaning of the colors is same as that in Fig. 1.

wall $x = L_x$ in an early stage [Figs. 3(b) and 4(b)], particles on the wall $x = L_x$ are ordered better than those on the wall $z = L_z$ in the late stage [Figs. 3(d) and 4(d)].

We also see the process of ordering of particles with a tilted angle. Figure 5 shows the snapshots of particles attaching to the top wall. In a very early stage [Fig. 5(a)], particles attach to the wall randomly. Some particles are accidentally ordered, but almost all of particles are disordered. With increasing time, the density of particles increases, and ordering on the wall starts around the edge $x = L_x$ and at the center of the wall [Fig. 5(b)]. Around $x = L_x$, the particles align parallel to the side and form triangle lattices, but at the center of the wall, the triangle lattice is rotated about 30° from $x = L_x$. The number of ordered particles increases with time [Fig. 5(c)], and in the last stage, almost all of the wall is occupied by the two types of ordered domains.

Figure 6 shows the snapshots of particles attaching on the wall $x = L_x$. Since the x component of the external force is as large as the z component, the wall is equivalent to the wall $z = L_z$. However, ordering is different from that on $z = L_z$: The top wall $z = L_z$ is covered with two types of ordered domains, but the side wall $x = L_x$ is covered with a single domain of red particles. In Fig. 5(d), the line of disordered particles is formed between the two types of domains. The system size is not so large in our simulation; once the a linear dislocation, which is as large as the system size, is formed, the dislocation is stable. If we wait for a long time, the dislocation probably vanishes. Then, reconstruction may occur and whole of the wall is covered by red particles.

To estimate ordering of the whole of a wall, we introduce $\langle\bar{\psi}\rangle$, which is the average of ψ_k over the whole surface and many runs. Figure 7 shows the time evolutions of $\langle\bar{\psi}\rangle$ averaged over 40 runs. The system size and the number of particles are larger than those in Fig. 1: The system is about $L_x = L_y = L_z = 41$ and the number of particles is $N = 13500$. We

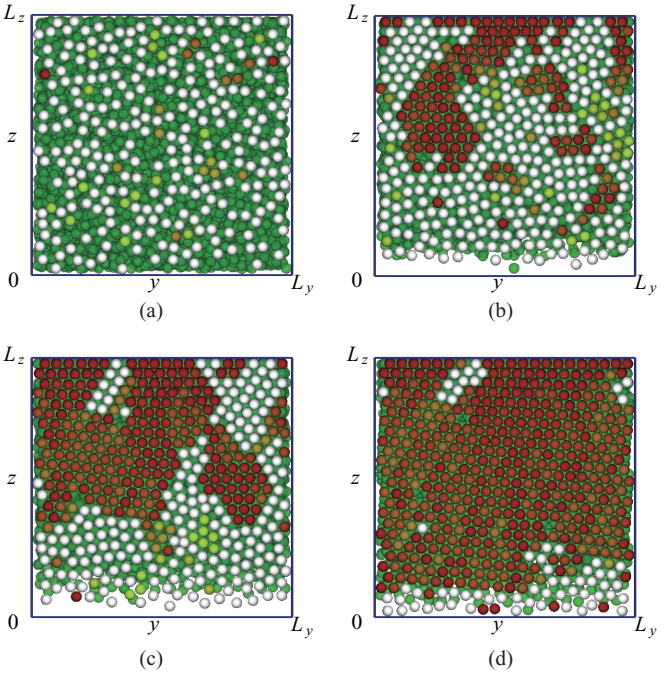

FIG. 6. (Color online) Snapshot of particles on the $x = L_x$ wall with the force $(1,0,1)/\sqrt{2}$. Particles with local sixfold orientational symmetry are colored. The meaning of the colors is same as that in Fig. 1.

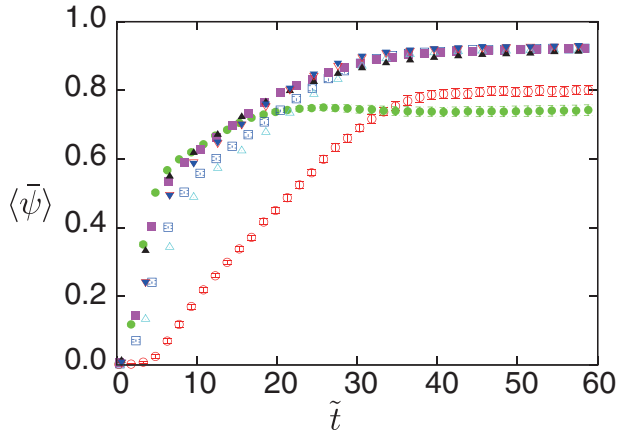

FIG. 7. (Color online) Time evolution of $\langle\bar{\psi}\rangle$. Open circles, solid circles, open squares, solid squares, open triangles, solid triangles, open inverted triangles, and solid inverted triangles show the time evolutions of $\langle\bar{\psi}\rangle$ on $z = L_z$ with the force $(0,0,1)$, $x = L_x$ with the force $(0,0,1)$, $z = L_z$ with the force $(1,0,\sqrt{2})/\sqrt{3}$, $x = L_x$ with the force $(1,0,\sqrt{2})/\sqrt{3}$, $z = L_z$ with the force $(1,0,\sqrt{3})/2$, $x = L_x$ with the force $(1,0,\sqrt{3})/2$, $z = L_z$ with the force $(1,0,1)/\sqrt{2}$, and $x = L_x$ with the force $(1,0,1)/\sqrt{2}$, respectively.

use four types of the external forces, $(0,0,1)$, $(1,0,\sqrt{2})/\sqrt{3}$, $(1,0,\sqrt{3})/2$, and $(1,0,1)/\sqrt{2}$, and estimate $\langle\bar{\psi}\rangle$ on $z = L_z$ and $x = L_x$.

In each case, on both walls $\langle\bar{\psi}\rangle$ increases with time in the initial stage and finally saturates. When the external force is $(0,0,1)$, the x component of the external force is 0. Ordering on $z = L_z$ occurs faster than that on $x = L_x$, but the saturated value of $\langle\bar{\psi}\rangle$ on $z = L_z$ is smaller than that on $x = L_x$. When the external force is tilted, the x component of the external force is present. When the direction of the external force is $(1,0,1)/\sqrt{2}$, the z component of the external force is as large as the x component. The data of the two walls overlap each other, so we cannot distinguish them in Fig. 7. With other angles, the z component of the external force is larger than the x component, so ordering on $z = L_z$ occurs faster than that on $x = L_x$ in the initial stage, which is similar to ordering with the force $(0,0,1)$. However, the saturated value of $\langle\bar{\psi}\rangle$ on $z = L_z$ is as large as that on $x = L_x$, which is different from the case with the force $(0,0,1)$. The saturated values of $\langle\bar{\psi}\rangle$ with the tilted forces are larger than those with the force $(0,0,1)$. From the results, the saturated value of $\langle\bar{\psi}\rangle$ seems to be independent of the tilting angle.

Since ordering probably occurs on walls at first, ordering in bulk is affected by that on walls. To estimate the order in bulk, we calculate orientation order parameters $Q_l(i)$, $\bar{Q}_l(i)$, and $w_l(i)$ [25,26], which represent the local orientation order around the ith particle. $Q_l(i)$ is defined as

$$Q_l(i) = \sqrt{\frac{4\pi}{(2l+1)}\sum_{m=-l}^{l}|q_{l,m}(i)|^2}, \tag{8}$$

where

$$q_{l,m}(i) = \frac{1}{n_{\rm n}}\sum_{j=1}^{n_{\rm n}} Y_l^m(\theta_{ij},\phi_{ij}). \tag{9}$$

The angles θ_{ij} and ϕ_{ij} represent the polar angle and the azimuthal angle of $\boldsymbol{r}_{ij}$, respectively. $Y_l^m(\theta_{ij},\phi_{ij})$ is the spherical harmonics and $n_{\rm n}$ is the number of neighboring particles. In the calculation of ψ_k in order to investigate the order of particles attaching on walls, we regarded the particles within $1.2r_{\rm in}$ as the neighboring particles, but we use a tighter condition in order to investigate ordering in bulk: The cutoff length is $1.1r_{\rm in}$. The parameter $w_l(i)$ is defined as

$$w_l(i) = \frac{\sum_{m_1+m_2+m_3=0}\begin{pmatrix} l & l & l \\ m_1 & m_2 & m_3\end{pmatrix} q_{l,m_1}(i)q_{l,m_2}(i)q_{l,m_3}(i)}{\left(\sum_{m=-l}^{l}|q_{l,m}(i)|^2\right)^{3/2}}, \tag{10}$$

where the integers m_1, m_2, and m_3 run from $-l$ to l and satisfy the condition $m_1 + m_2 + m_3 = 0$, and the term in the parentheses is the Wigner 3-j symbol.

The parameters $Q_l(i)$ and $w_l(i)$ hold the information of the structure of the first shell around the ith particle. To take account of the second-order shell and to increase the accuracy of the distinction of the difference in structure around the ith particle, $\bar{Q}_l(i)$ is introduced. The definition of $\bar{Q}_l(i)$ is given by

$$\bar{Q}_l(i) = \sqrt{\frac{4\pi}{(2l+1)}\sum_{m=-l}^{l}|\bar{q}_{l,m}(i)|^2}, \tag{11}$$

where

$$\bar{q}_{l,m}(i) = \frac{1}{\tilde{n}_{\rm n}}\sum_{j=0}^{\tilde{n}_{\rm n}} q_{l,m}(j). \tag{12}$$

In Eq. (12), the sum from $j = 0$ to $\tilde{n}_{\rm n}$ runs over all neighbors of the ith particle plus the particle itself.

Figure 8 shows the distributions of the hcp structure and the fcc structure on parameters plane, where we use the data in Fig. 2(d). We regard the structure of particles with $w_4 > 0.01$ and $Q_4 < 0.15$ as the hcp structure and that with $w_4 < -0.02$ and $Q_4 > 0.15$ as the fcc structure. In calculating order parameters, we neglected the particles which do not have 12 nearest neighbors. Thus, particles with the bcc structure and almost all of the disordered particles are excluded, which is consistent with the distribution of points in the Q_4-Q_6 plane. The distribution of two structures in the Q_4-Q_6 plane also do not contradict the expected form [26–29].

In Fig. 9, we use the data in Fig. 1 and show the positions of particles with 12 nearest neighbors in bulk. Particles with the local hcp structure are colored yellow (light gray), those with the local fcc structure are colored cyan (dark gray), and the others are colored white. In a very early stage [Fig. 9(a)], the particles with 12 neighbors appear near $z = L_z$ uniformly. They form small domains of the fcc structure and the hcp structure. With increasing time [Fig. 9(b)], the number of the particles increases along side walls. Then, the thickness of domains increases. In Fig. 9(c), the thickness of domains increases from both the side walls and the top wall. In the final stage [Fig. 9(d)], we can find that the layerlike domains with the hcp structure and the fcc structure, which are parallel to the size wall $x = L_x$, appear.

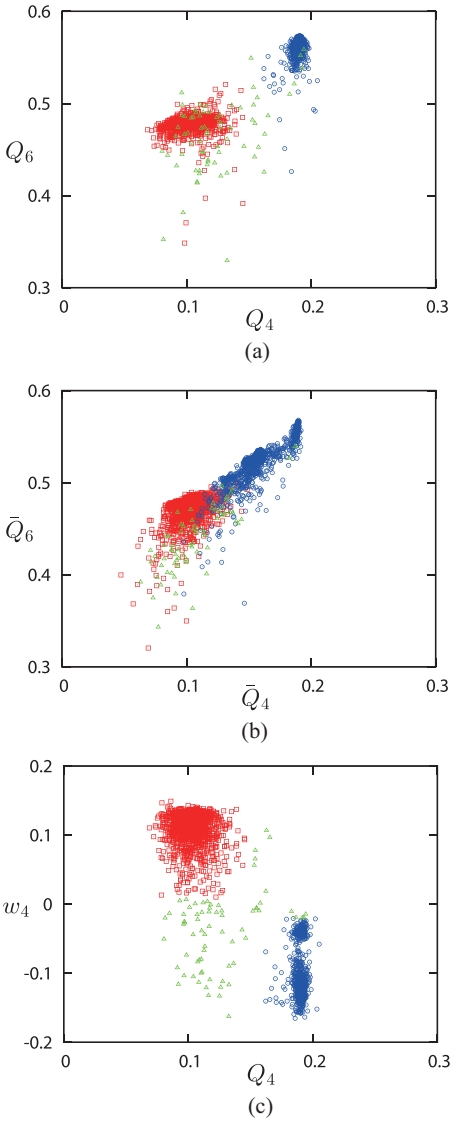

FIG. 8. (Color online) Distribution of hcp structure and fcc structure in (a) the Q_6-Q_4 plane, (b) the $\bar{Q}_6$-$\bar{Q}_4$ plane, and (c) the w_4-Q_4 plane. Red open squares, blue open circles, and green open triangles represent the particles with hcp structure, fcc structure, and disordered structure, respectively. We use the data in Fig. 2(d).

Figure 10 shows snapshots of the local structure with the force $(1,0,1)/\sqrt{2}$. When the direction of the force is tilted, ordering of particles occurs from the side line between $x = L_x$ and $z = L_z$. In an early stage (Fig. 10), the particles with 12 neighbors appear along the two walls. Thin two-dimensional domains with the hcp structure mainly appear near the side wall $x = L_x$ and those with the fcc structure mainly appear near the top wall $z = L_z$. In Fig. 10(b), the two-dimensional layers spread. While the side wall $x = L_x$ is mainly filled with the domain with the hcp structure, the two types of domains are formed on the top wall $z = L_z$. Then, the thickness of ordered particles increases. In Figs. 10(c) and 10(d), the thickness seems to increase from the side wall.

We also study how the distribution of cluster size changes with the direction of the external force. Figure 11 shows the

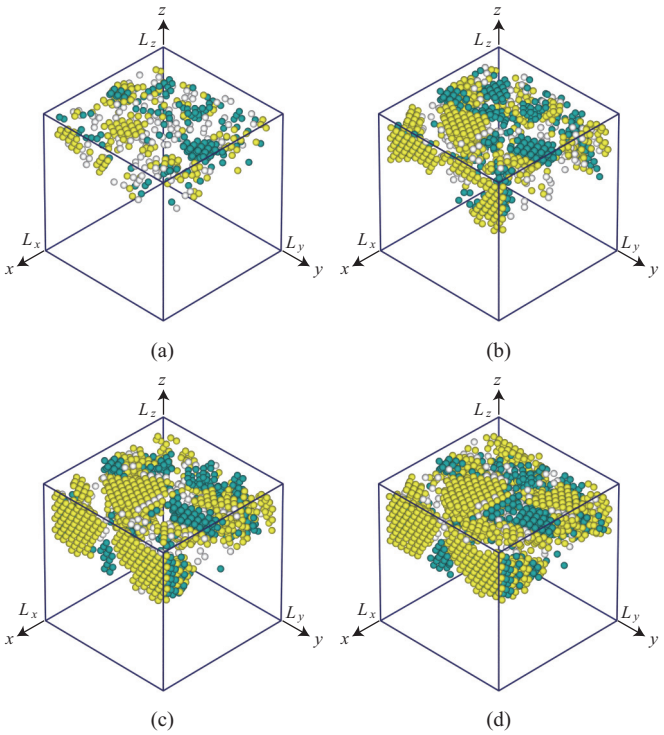

FIG. 9. (Color online) Snapshots of positions of particles with the local hcp structure and the local fcc structure. We use the data in Fig. 1. The structures around yellow (light gray) particles, cyan (dark gray) particles, and white particles are hcp, fcc, and the other, respectively. Time is (a) $\tilde{t} = 12$, (b) $\tilde{t} = 24$, (c) $\tilde{t} = 40$, and (d) $\tilde{t} = 80$.

dependence of the number of clusters $N_{\rm nc}$ on the cluster size $n_{\rm c}$. The system size and the number of particles are the same as those in Fig. 7, and we check the distributions in the final stage with averaging over 40 runs. The average numbers of the ordered particles with the fcc structure and the hcp structure are 2647 and 4398, respectively. The number of particles with the hcp structure is larger than that with the fcc structure. When the direction of the external force is perpendicular to $z = L_z$ [Figs. 11(a) and 11(b)], a lot of small clusters are formed and large clusters do not appear. Figures 11(c) and 11(d) show the distribution of the cluster size with the external force $(1,0,\sqrt{2})/\sqrt{3}$. The increase of numbers of the ordered particles is small: The average numbers of the ordered particles with the fcc structure and the hcp structure are 3278 and 4631, respectively. The difference of the numbers of particles in two structures decreases and large clusters, which do not appear with the external force perpendicular to the top wall $z = L_z$, are formed with a tilted external force. Decrease in the number of very small clusters ($n_{\rm c} < 100$) is small, but the number of middle size clusters ($100 < n_{\rm c} < 1000$) decreases and the number of large size clusters increases.

IV. SUMMARY

In this paper, to keep the formation of colloidal crystals under the centrifugation force in mind, we studied the formation of a crystal of Brownian particles under a uniform external force. When the external force is added in the system,

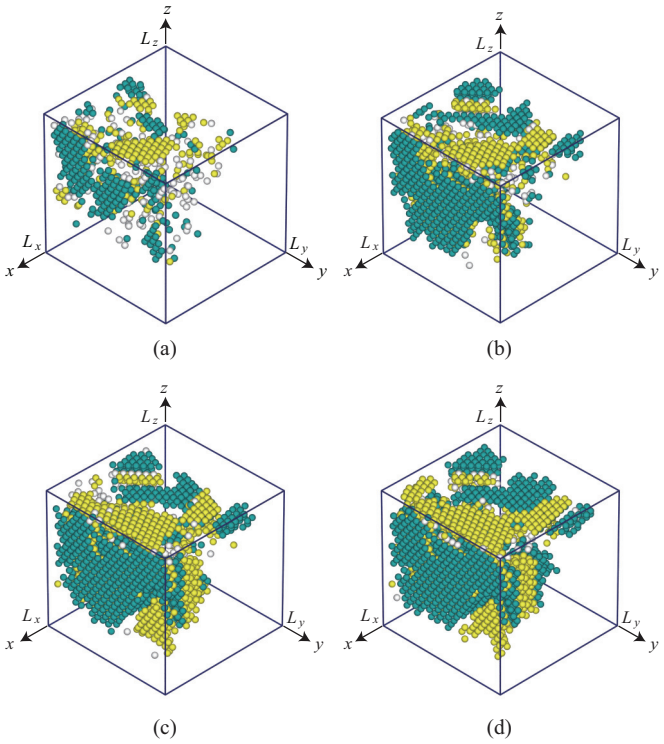

FIG. 10. (Color online) Snapshot of positions of particles with hcp structure and fcc structure. We use the data in Fig. 2. The mean of color of particles is same as that in Fig. 9 Times in (a)–(d) are the same as those in Figs. 9(a)–9(d).

the density of particles near walls increases and crystallization occurs. When the uniform external force is perpendicular to a wall, the whole wall becomes occupied by particles. The reconstruction in the wall is difficult because there is no extra space for particles to move for reconstruction. On the other hand, if the external force is tilted, the density first

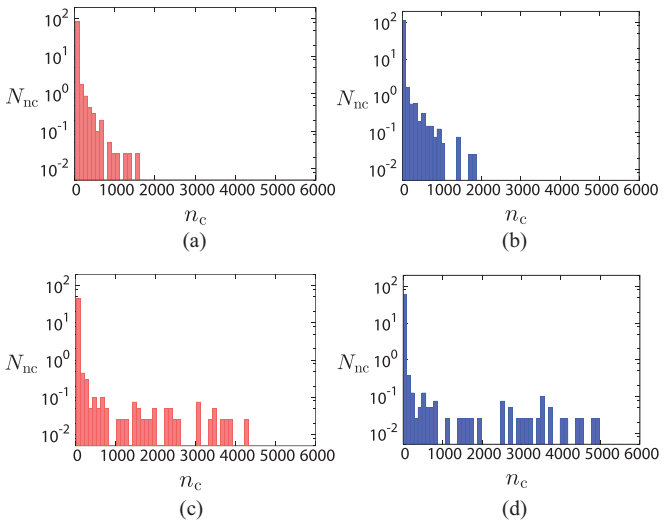

FIG. 11. (Color online) Dependence of number N_{nc} of clusters whose size is n_c. The external force is (0,0,1) in (a) and (b) and $(1,0,\sqrt{2})/\sqrt{3}$ in (c) and (d). Panels (a) and (c) show the dependence of fcc clusters, and (b) and (d) show that of hcp clusters. The data are averaged over 40 runs.

increases around an edge. The density around an edge in the other side is low, so that the particles, which attach to the wall, can move easily and the reconstruction occurs. Thus, with the tilted force, ordering of particles on walls is better than that with perpendicular force. From our simulation, we investigated $\langle\bar{\psi}\rangle$ with a few tilting angles. We cannot judge whether $\langle\bar{\psi}\rangle$ with the perpendicular force is singular or not. There may be a threshold of the tilting angle which induces the increase of $\langle\bar{\psi}\rangle$, so we need to investigate $\langle\bar{\psi}\rangle$ with various angles.

Ordering in bulk is related to that on a wall because crystallization starts on walls. Ordering in bulk with tilted force is better than that with perpendicular force: The number of ordered particles increases and the size of the domain enlarges with tilted force. In our simulation, the system size is small and the potential between particles is probably less complicated than that between colloidal particles in experiment, so that we cannot compare our results with the experiments quantitatively. However, our result that grain size increases by tilted external force qualitatively agrees with experiments [11,12].

In experiment [30], although the random hexagonal close-packed (rhcp) structure is formed under microgravity, the fcc structure and the rhcp structure are mixed under normal gravity, which shows that the gravity seems to enhance the formation of fcc structure. To create a good template for inverse opals [1], it is necessary to produce large domains with the fcc structure. However, in our simulation, the domains with the local fcc structure and the local hcp structure are mixed, which is probably because the external force and the density of particles are larger than the value used in previous studies [16–19]. In the experiment [12], silica particles of 110 nm were used. The acceleration of the centrifugal force was 22 m/s^2 and temperature was 30 °C. Since the density of silica is 2.65 g/cm^3, the Peclet number is estimated to be 1.07×10^{-3}, which is much smaller than the Peclet number in our simulation. Since the initial density of particles or the drift velocity caused by the external force is large in our simulation, crystal grows before it relaxes to a suitable state, and the small domains of the hcp structure and the fcc structure appear. If we carry out simulation with a low density of particles and a small external force, crystal with large domains of fcc structure may be formed.

Recently, Mori and co-workers [10] carried out Monte Carlo simulation with hard sphere particles and showed that defects in polycrystal vanished by controlling the strength of gravitational force. Even in our model, we may be able to enlarge the size of domain with the local fcc structure by controlling the strength of gravitational force after forming a polycrystal. Thus, we also try to study how the ordering in bulk changes with the strength of the uniform force.

ACKNOWLEDGMENTS

This work is supported by Grants-in-Aid for Scientific Research from Japan Society for the Promotion of Science, and some parts of this study were carried out under the Joint Research Program of the Institute of Low Temperature Science, Hokkaido University.

[1] A. Blanco, E. Chomski, S. Grabtchak, M. Ibisate, S. John, S. W. Leonard, C. Lopez, F. Meseguer, H. Miguez, J. P. Mondia, G. A. Ozin, O. Toader, and H. M. Van Diel, Nature (London) **405**, 437 (2000).
[2] L. Thylen, M. Qiu, and S. Anand, Chem. Phys. Chem. **5**, 1268 (2004).
[3] T. Sawada, Y. Suzuki, A. Toyotama, and N. Iyi, Jpn. J. Appl. Phys. **40**, L1226 (2001).
[4] T. Kanai, T. Sawada, A. Toyotama, and K. Kitamura, Adv. Funct. Mater. **15**, 25 (2005).
[5] J. Yamanaka, M. Murai, Y. Iwayama, M. Yonese, K. Ito, and T. Sawada, J. Am. Chem. Soc. **126**, 7156 (2004).
[6] A. Toyotama, J. Yamanaka, M. Yonese, T. Sawada, and F. Uchida, J. Am. Chem. Soc. **129**, 3044 (2007).
[7] Y. Yin, Z. Li, and Y. Xia, Langmuir **19**, 622 (2003).
[8] K. E. Davis, W. B. Russel, and W. J. Glantschnig, Science **245**, 507 (1983).
[9] A. Mori, S. Yanagiya, Y. Suzuki, T. Sawada, and K. Ito, J. Chem. Phys. **124**, 174507 (2006).
[10] A. Mori, Y. Suzuki, and S. Matsuno, Chem. Lett. **41**, 1069 (2012).
[11] Y. Suzuki, T. Sawada, and K. Tamura, J. Cryst. Growth **318**, 780 (2011).
[12] K. Hashimoto, A. Mori, K. Tamura, and Y. Suzuki, Jpn. J. Appl. Phys. **52**, 030201 (2013).
[13] A. J. Page and R. P. Sear, Phys. Rev. Lett. **97**, 065701 (2006).
[14] J. D. Weeks, D. Chandler, and H. C. Anderson, J. Chem. Phys. **54**, 5237 (1971).
[15] D. L. Ermak, J. Chem. Phys. **62**, 4189 (1975).
[16] H. Mèguez, F. Meseguer, C. López, A. Misfud, J. S. Moya, and L. Vázquez, Langmuir **13**, 6009 (1997).
[17] P. Hoogenboom, D. Derks, P. Vergeer, and A. van Blaaderen, J. Chem. Phys. **117**, 11320 (2002).
[18] J. Hilhorset, J. R. Wolters, and A. V. Petukhov, Cryst. Eng. Commun. **12**, 3820 (2010).
[19] M. Marechal, M. Hermes, and Marjolein Dijkstra, J. Chem. Phys. **135**, 034510 (2011).
[20] A. Mori, Y. Suzuki, and S. Yanagiya, Fluid Phase Equilib. **257**, 131 (2007).
[21] B. I. Halperin and David R. Nelson, Phys. Rev. Lett. **41**, 121 (1978).
[22] R. Yamamoto and A. Onuki, J. Phys. Soc. Jpn. **66**, 2545 (1997).
[23] R. Yamamoto and A. Onuki, Phys. Rev. E **58**, 3515 (1998).
[24] T. Hamanaka and A. Onuki, Phys. Rev. E **74**, 011506 (2006).
[25] P. J. Steinhardt, D. R. Nelson, and M. Ronchetti, Phys. Rev. B **28**, 784 (1983).
[26] W. Lechner and C. Dellago, J. Chem. Phys. **129**, 114707 (2008).
[27] C. Desgranges and J. Delhommelle, Phys. Rev. B **77**, 054201 (2008).
[28] M. D. Rintoul and S. Torquato, J. Chem. Phys. **105**, 9258 (1996).
[29] A. Panaitescu, K. A. Reddy, and A. Kudrolli, Phys. Rev. Lett. **108**, 108001 (2012).
[30] J. Zhu, M. Li, R. Rogers, W. Meyer, R. H. Ottewill, STS-73 Space Shuttle Crew, W. B. Russel, and P. M. Chaikin, Nature (London) **387**, 883 (1997).